Trans Indian Inst Met
DOI 10.1007/s12666-017-1197-4

TECHNICAL PAPER

Effect of Bonding Temperature on Microstructure and Mechanical Properties of WC–Co/Steel Diffusion Brazed Joint

Mahdi Shafiei Haghshenas[1] · **Nader Parvin**[1] · **Ali Amirnasiri**[1]

Acknowledgements We thank Taradis Tabesh Azma and CylinderSazi Tehran companies for support of this research.

Received: 9 November 2016 / Accepted: 28 August 2017

Abstract In this work, the diffusion brazing of AISI 4145 steel to WC–Co cemented carbide using RBCuZn-D interlayer with bonding temperature values of 930, 960, 990 and 1020 °C was studied. The microstructure of the joint zone was evaluated by scanning electron microscope (SEM) and X-ray diffraction (XRD). Vickers microhardness and shear strength tests were performed to investigate mechanical behaviors of the brazed joints. The XRD and SEM results indicated that with increase of bonding temperature, the elements readily diffused along the interface and formed various compounds such as γ, α and β and Co_3W_3C. The results also showed that with the increase of bonding temperature from 930 to 960 °C, a sound metallurgical bond was produced, however in higher bonding temperatures (990 and 1020 °C) a decrease in mechanical properties of the joints was observed which could be due to the excessive zinc evaporation, interface heterogeneity and voids formation. The maximum shear strength of 425 MPa was obtained for the bond made at 960 °C.

Keywords WC–Co · 4145 Steel · Diffusion · Joining · Microstructure

1 Introduction

WC–Co cemented carbides are widely exploited for many applications such as press molds, mining bits, tempting machines, hydraulic components and drilling [1–5]. In these alloys, a high fraction of WC particles is embedded in a tough Co binder to produce a multiphase material with superior wear resistance, high hardness and strength. Nonetheless, the high cost and the low plasticity confine the extensive use of this material in many industries. To tackle these problems, researchers have tried to employ WC–Co cemented carbide in combination with other alloys such as steels to fabricate intricate configurations for various applications [6, 7]. However, great differences in physical properties of these alloys like thermal conductivity, residual stress generation and linear expansion coefficient creates firm barriers to employing WC–Co and steel together [8]. Hence, advanced joining processes have taken a widespread interest to attain a sound WC–Co/steel joint [9–16]. Among them, brazing technique has been selected as one of the main processes for bonding of WC–Co/steel so that the couple resists to high mechanical loading and preserves its essence for a long working time [17, 18]. Nowacki and Kawiak [19] investigated vacuum brazing of WC–Co to 17-4 PH steel for large-dimension-spinning nozzles. They determined that the thickness of the filler metal had essential impact on the local stress values and the joint rigidity. The induction brazing of WC–Co/steel system using Ag–Cu based interlayer was performed by Jiang et al. [20]. It was found that the distribution of α-Cu solid solution phases at the interface played a vital role in strengthening mechanism of the bond. Moreover, the increase of bonding temperature led to a reduction in total area of strengthening phase in the joint zone and subsequently the decrease in mechanical properties of the brazed joint. Li et al. [21] performed hybrid ultrasonic induction brazing of WC–Co/35CrMo steel using Ag–Cu–Zn–Mn–Ni filler metal. It was reported that WC particles were well distributed in the joint zone by the ultrasonic-assisted brazing technique and remarkably increased the tensile

✉ Ali Amirnasiri
ali.amirnasiri@yahoo.com; arvin@aut.ac.ir

[1] Faculty of Mining and Materials Engineering, Amirkabir University of Technology (AUT), Tehran, Iran

strength of brazed joints. It was also noticed that the ultrasonic vibration significantly affected the wettability of Ag-based filler metal at the interface. The brazed joints of stainless steel and WC–Co using Ni electroplated on Cu–Zn alloy as interlayer were studied [22]. It was concluded that the deposited Ni promoted the formation of reaction zone and possessed a positive impact on the mechanical behaviors of the joint. Cu–Mn–Zn filler metal was also used as interlayer to join WC–Co/steel couple [23]. The results indicated that the filler metal efficiently wetted both steel and cemented carbide and produced a sound metallurgical bond.

According to the literatures, Cu–Zn based alloys can be promising alternatives for high cost Ag-based brazing filler metals when high-temperature work services are needed [22–26]. Thus the objective of the present work is to investigate the influence of filler metal characteristics (Cu–Zn based alloy) on microstructure and mechanical behaviors of the brazed joint and achieve the optimum processing parameters by varying bonding temperature as a main factor.

2 Materials and Methods

The parent materials used in this work were AISI 4145 steel (0.47 C–0.25 Ni–0.94 Mn–0.88 Cr–0.22 Mo–0.24 Si–bal. Fe) and WC–Co (3.98 C–10.87 Co–0.24 Nb–bal. W), which were cut into dimensions of $3 \times 5 \times 12.5$ mm^3 coupons. RBCuZn-D foil (52.5 Cu–37.9 Zn–9.6 Ni) with the thickness of 150 μm and the melting point of 920 °C was applied to produce a brazed joint. At first, the surface of parent materials were prepared on SiC paper to a 400 grit finish. The interlayer foil was held between the samples and the assembly was then transferred to the furnace chamber under vacuum of 10^{-3} mBar. A pressure of 0.2 MPa was employed to the bonding surfaces to fix the assembly. The diffusion brazing process was conducted in an induction furnace with heating rate of 40 K/s, bonding time of 10 min and temperature values of 930, 960, 990 and 1020 °C.

After bonding process, the cross sections of brazed joints were provided for metallographic evaluation using standard polishing methods. The chemical etchant for the cemented carbide side was Murakami solution [27] and steel was etched by nital reagent (2 vol% HNO_3) [27]. The microstructure was analyzed by scanning electron microscopy (SEM) equipped with an energy dispersive spectrometer while the phase constitution was studied by X-ray diffraction (XRD). To assess the mechanical properties of brazed joints, the shear strength was measured based on ASTM standard D1002-99 [28]. Hardness measurement was also performed by Leco tester with a load of 500 g and 15 s load time.

Sessile drop technique was used to study the wettability of filler metal. In the wettability test, the substrate (WC–Co) was removed from oxide film and washed by acetone. The 50 g filler metal with the granular shape was placed on the substrate and then the system was put into the vacuum furnace with processing temperature of 930, 960, 990, 1020 °C. The last step was the measurement of wetting angle using a digital camera and Image J software.

3 Results and Discussion

3.1 Wettability of Cemented Carbide

Figure 1 displays wetting and spreading behavior of molten RBCuZn-D on the cemented carbide at different brazing temperature. In general, the filler metal has good wettability on the WC–Co alloy. The left/right wetting angles at 930 °C are estimated about 39°/31°. With the increase of brazing temperature up to 960 °C, the wetting angles decreases dramatically (31°/25°) and as a result, the wettability of brazing filler metal get modified. In fact, the decrease of wetting angle indicates that the enhancement of temperature leads to the improvement of wettability. Thereafter, the increase of temperature has a slight effect on the wettability so that it just reduces to 24°/29° and 21°/27° at 990 and 1020 °C, respectively.

3.2 Effect of Bonding Temperature on Microstructure

SEM micrograph of the brazed bond made at 930 °C is illustrated in Fig. 2. The joint is free from structural defects like cracks and voids. The linear shape of interfaces at WC–Co and steel sides indicates low interdiffusion of elements across the joint zone. As shown in Fig. 2b, there is no sign of reaction layer in the joint zone at WC–Co side. This can be owing to the low bonding temperature which does not give a chance to the elements to migrate along the interface. The EDS spectra in region A confirms that a negligible amount of elements from WC–Co diffuses into the filler metal (see Table 1). Figure 3 shows the SEM micrograph of the bond made at 960 °C. The interlayer consists of two separated regions. Based on EDS analysis and Cu–Ni–Zn ternary phase diagram [29], region B is defined as α-Cu solid solution phase. However Ni shows a strong affinity towards this phase. Region C, placed among α phase, mainly contains Zn element indicating the formation of β Zn-rich solid solution phase. It is suggested that during solidification of interlayer in the bonding process, zinc exits from α phase and forms a distinct phase (β)

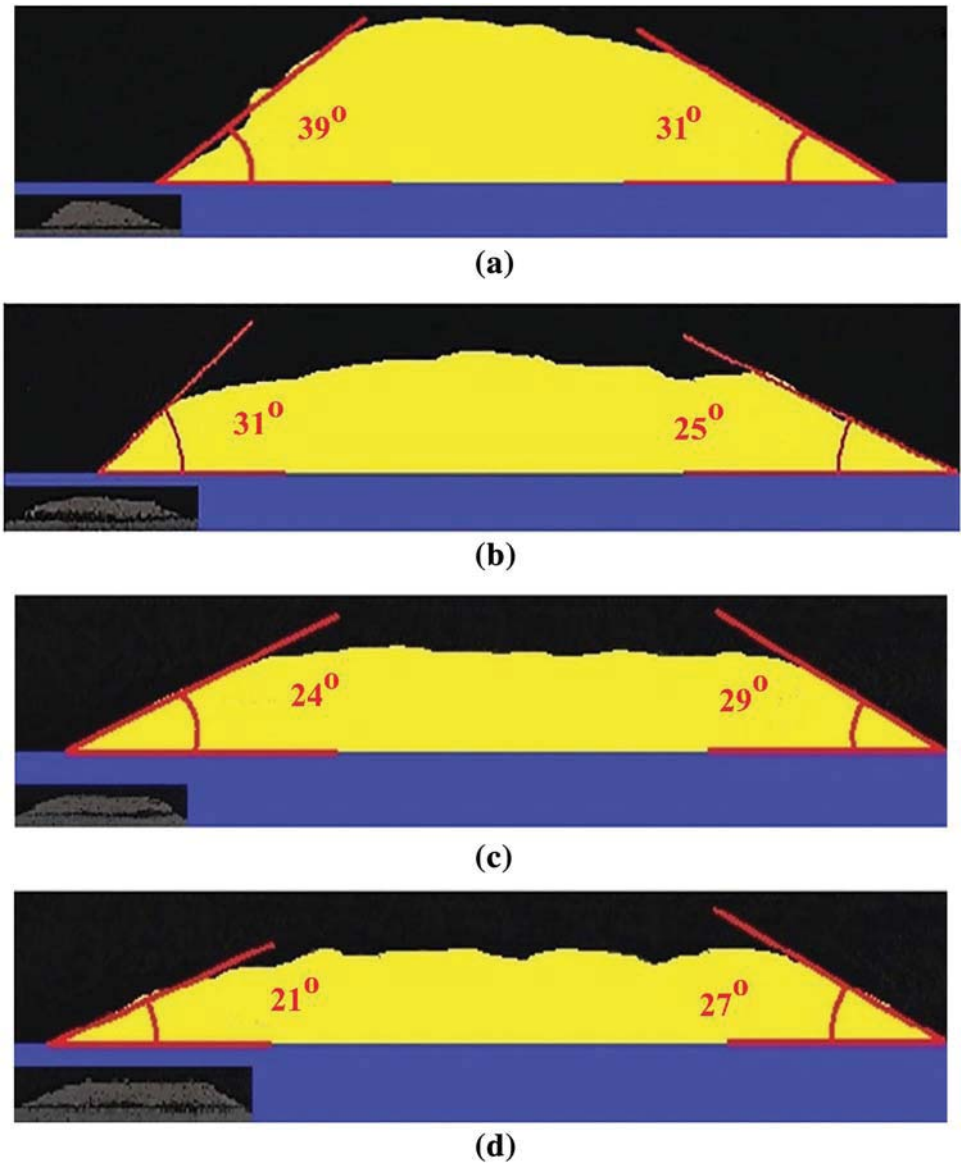

Fig. 1 Spreading behavior of molten RBCuZn-D on the cemented carbide at **a** 930 °C, **b** 960 °C, **c** 990 °C, **d** 1020 °C

at the center of joint zone. It should be noted that the mutual exclusion between Ni and Zn leads to the migration of Ni outward the β phase. Moreover, small area of β phase at the joint center can be due to the zinc evaporation and subsequent drop of this element at the interface. Figure 3b shows that some sporadic regions are created at the steel interface. Based on the EDS results, the great affinity of Ni for Fe leads to the enrichment of Ni adjacent to the steel and the formation of γ phase (austenite) at the interface [22]. It is also seen that a diffusion layer is formed along the cemented carbide. The interlayer infiltrates and reacts with cemented carbide and creates a diffusion layer with thickness of 40 μm at the interface. In fact, substantial diffusivity of Ni in Co is the main reason for development of reaction layer at WC–Co side. So one can conclude that Ni in the interlayer plays an important role in generation of the reaction layers in the joint zone. High-magnification of micrograph of interfacial structure at the WC–Co side indicates that some WC particles get detached from the base material and are released into the interlayer. This noteworthy phenomenon is associated with high solubility of Co into the interlayer. It means that Co is readily dissolved in the liquid filler metal and as a result, the cemented carbide adjacent to the interface is depleted from Co as binder. Hence, the WC particles can be easily separated from each other and distributed near the interface. As observed, this phenomenon results in the creation of a non-linear structure at the interface and the enhancement of contact area between the joint zone and WC–Co.

Figure 4 demonstrates the SEM micrograph of a bond made at 990 °C. As shown, increase of bonding temperature to 990 °C intensifies the dissolution of Co into the

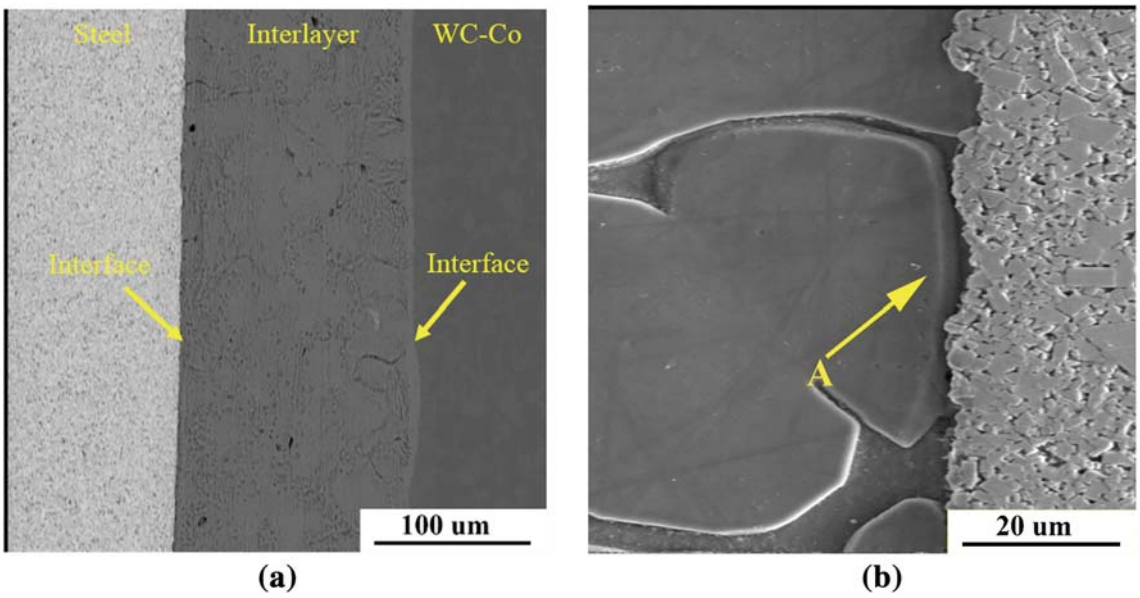

Fig. 2 SEM micrograph of a bond made at 930 °C, **a** joint zone, **b** WC–Co side

Table 1 EDS analysis (wt%) of marked regions in SEM micrographs

	Fe	C	Ni	Mn	Si	Cr	Mo	Co	W	Nb	Cu	Zn
A	0	0.07	19.41	0.01	0	0.02	0	0.7	0.03	0.03	70.32	9.41
B	0	0.03	22.81	0	0.02	0.01	0	0.02	0	0	71.59	5.53
C	0	0.01	4.21	0	0	0.03	0	0.02	0	0	41.91	53.32
D	0	0.10	16.31	0	0	0	0	12.27	0.18	0.7	57.93	12.51
E	0	9.83	0	0	0	0	0	0.1	89.97	0.07	0.03	0
γ	74.91	0.21	23.33	0.4	0.1	0.33	0.12	0.01	0	0	0.51	0.08

interlayer so that a considerable amount of WC particles is released from the base material and forms a reaction layer with thickness of 80 μm at the interface. For the bond made at 1020 °C (see Fig. 5), WC particles are unpleasantly dispersed in the joint zone. The bonding temperature is so high that the carbides can readily move inside the interlayer. Figure 5b shows the formation of some structural imperfection sticking to the WC particles. It is believed that the void formation can be attributed to the irregular shrinkage during joint solidification and stress induced growth by CTE mismatch between interlayer and free WC particles.

Figure 6 approves the evaporation of zinc element with the increase of bonding temperature. According to the regional EDS analysis, the zinc value in the center of the joint zone for the bond made in 930 °C is 35 wt% while for the bond made in 1020 °C, it decreases to less than 27 wt%. One can also see that the value of Co for the bond made in 1020 °C is more than that of the other sample. It shows the dissolution of Co from the cemented carbide into the interlayer.

3.3 Mechanical Analysis

Figure 7 illustrates the microhardness profiles for the brazed bonds made using RBCuZn-D interlayer for 10 min at 930, 960, 990 and 1020 °C. The first point one can see is the effect of joint width on distribution of hardness across the bonds. As shown in Fig. 7 and SEM micrographs, there is a straight relationship between the bonding temperature and the joint width so that the increase of bonding temperature to higher values lead to a dramatic rise in the width of joint zone. This can be observed apparently when one compares the hardness profile for the bond made at 930 °C with the hardness profile for the bond made at 1020 °C. The estimations indicate that the joint width with respect to bonding temperature is about 160, 210, 240 and 330, respectively.

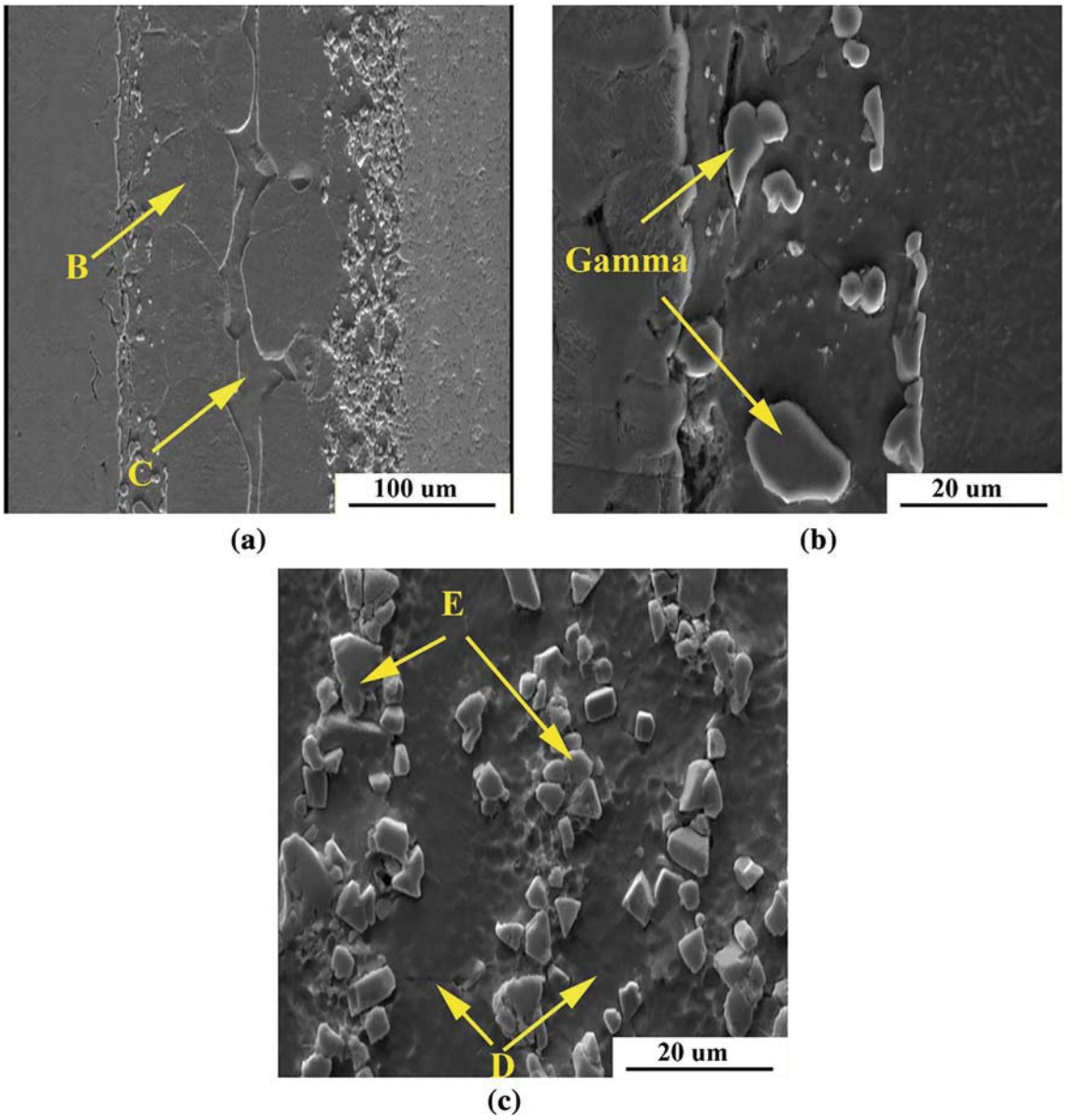

Fig. 3 SEM micrograph of a bond made at 960 °C, **a** joint zone, **b** steel side, **c** WC–Co side

The left side of the profiles for all the specimens shows the presence of cemented carbide with hardness value of 1550–1600 VHN. For the samples bonded at 960, 990 and 1020 °C, a slight drop in hardness ranging from 1100–1400 VHN is observed adjacent to WC–Co which can be due to the presence of a reaction layer at the interface. However, the steep slope in the profile of the bond made at 930 °C is attributed to the finite inter-diffusion of elements in this region and linear shape of the interface. The hardness values maintain the same level in the joint center which is due to the formation of α and β phases. Nevertheless, it can be seen that with increase of bonding temperature, the mean hardness value in this region moderately declines from 370 to 260 VHN. It is believed that zinc evaporation in higher bonding temperature along with diffusion of Ni towards the parent materials can be the main reason for decrease of hardness in this region. Approaching the steel, a sharp drop is observed for the bond made at 930 °C while a gradual decrease is found in this region for other specimens. It may be due to inter-diffusion of elements at higher temperature and formation of γ phase in the vicinity of 4145 steel.

The shear strength of joints as a function of bonding temperature is given in Fig. 8. The attained data reveals that increase of bonding temperature to 960 °C causes a boom in shear strength value. However it then decreases moderately. This indicates that an optimum bonding temperature is required to produce a sound metallurgical bond. The low

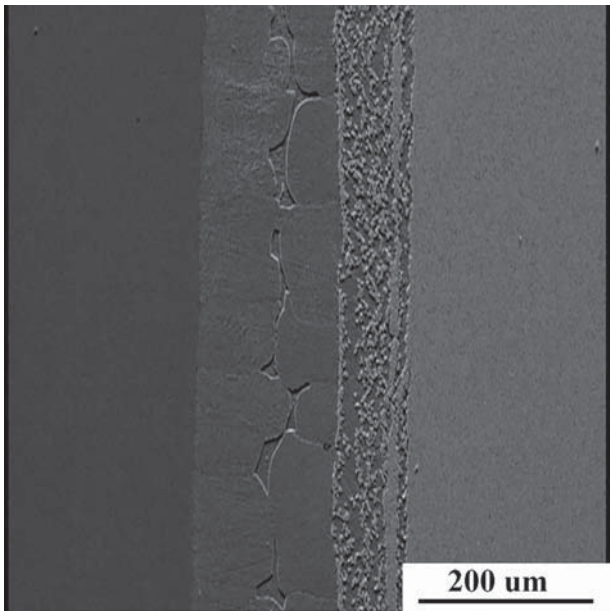

Fig. 4 SEM micrograph of a bond made at 990 °C

shear strength of the bond made at 930 °C can be attributed to the low inter-diffusion of elements across the joint zone and linear shape of interfaces. With increase of bonding temperature to 960 °C, the reaction layers are formed at the interfaces and the contact area between parent materials and interlayer increases and consequently the shear strength significantly improves. But when the bonding temperature rises to higher values, the diffusion layer in the vicinity of WC–Co becomes heterogeneous and uneven. Moreover, formation of imperfections sticking to the free WC particles in the joint zone can be another reason for a fall in the shear strength of the bonds made at higher temperature.

3.4 Fractogrphy

Figure 9 represents the fracture surface of bonded specimens caused by the shear strength test. For all the specimens, the failure as a result of shear force occurs within the joint zone near the cemented carbide. The weak interface of interlayer/WC–Co in the bond made at 930 °C lead to a catastrophic fracture along the joint zone. The presence of sticking WC particles on the fracture surface approves low atomic diffusion at the interface and crack propagation in this region. The fracture morphology is completely different for the bond made at 960 °C. One can see that with increase of bonding temperature and inter-diffusion of elements across the joint zone, an interwoven interface is formed and as a result, the crack propagation is impeded in this region. On the other hand, the significant atomic diffusion in this specimen results in the presence of α and β solid solution phases and free WC particles at the interlayer/WC–Co interface (Fig. 10b) and leads to the creation of pseudo-plastic fracture mode. With increase of bonding temperature to higher values, interface heterogeneity along with formation of voids sticking to the free WC particles changes the failure mode to a mixture of ductile fracture and brittle rupture. The free WC particles are apparently observed on the fracture surfaces in Fig. 9c, d.

Fractured surfaces of the bonds at WC–Co side have been analyzed using XRD. The results show that no intermetallic compounds are formed at the interface of the bond

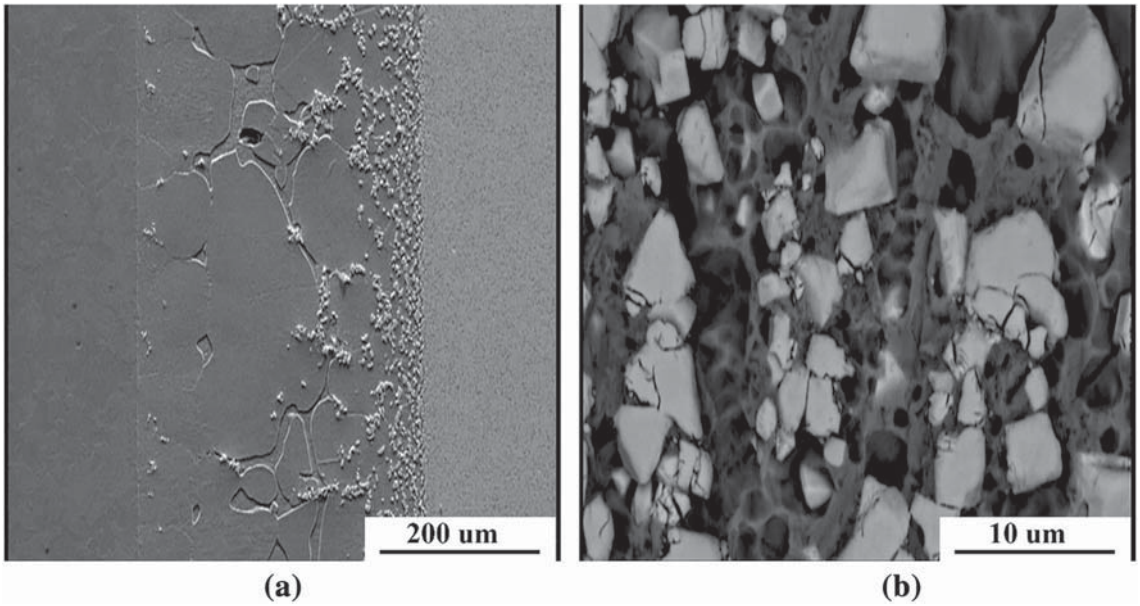

Fig. 5 SEM micrograph of a bond made at 1020 °C, **a** joint zone, **b** free WC particles

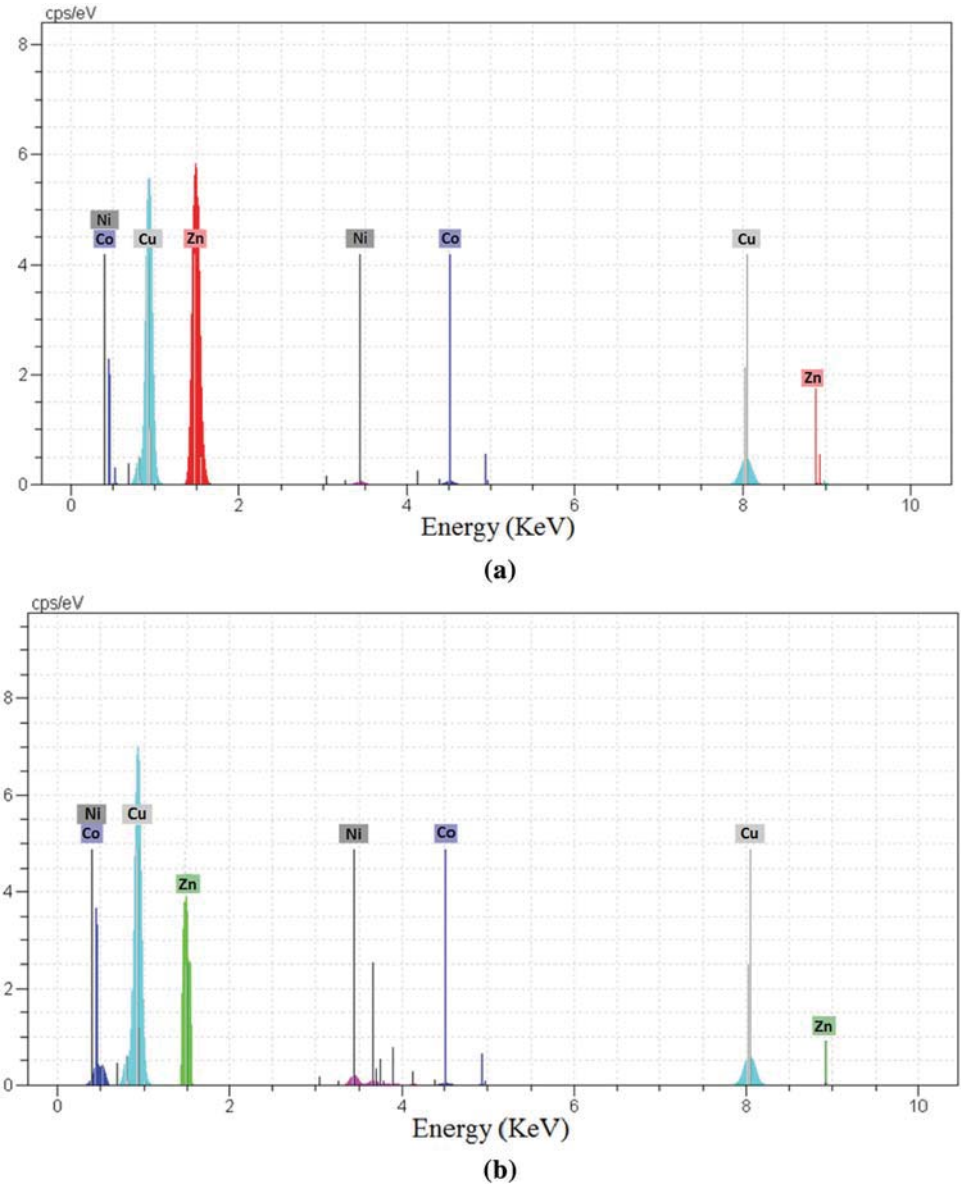

Fig. 6 EDS analysis from the joint center of the bonds made in **a** 930 °C, **b** 1020 °C. The chemical composition for **a** is 52 wt% Cu–36 wt%Zn–10 wt% Ni–2 wt% Co and for **b** is 56 wt% Cu–27 wt% Zn–9 wt% Ni–8 wt% Co

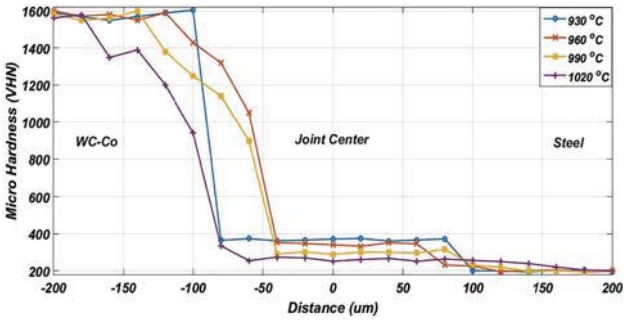

Fig. 7 Microhardness profiles for the bonds made at various bonding temperature

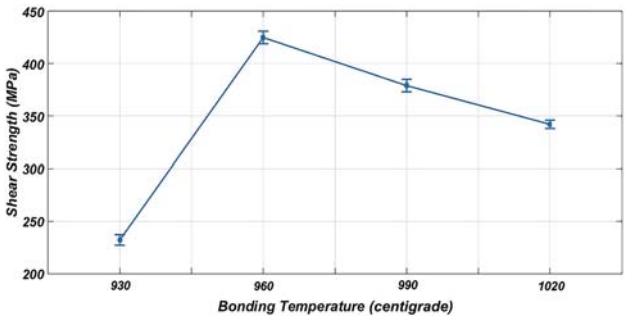

Fig. 8 Shear strength values for the bonds as a function of bonding temperature

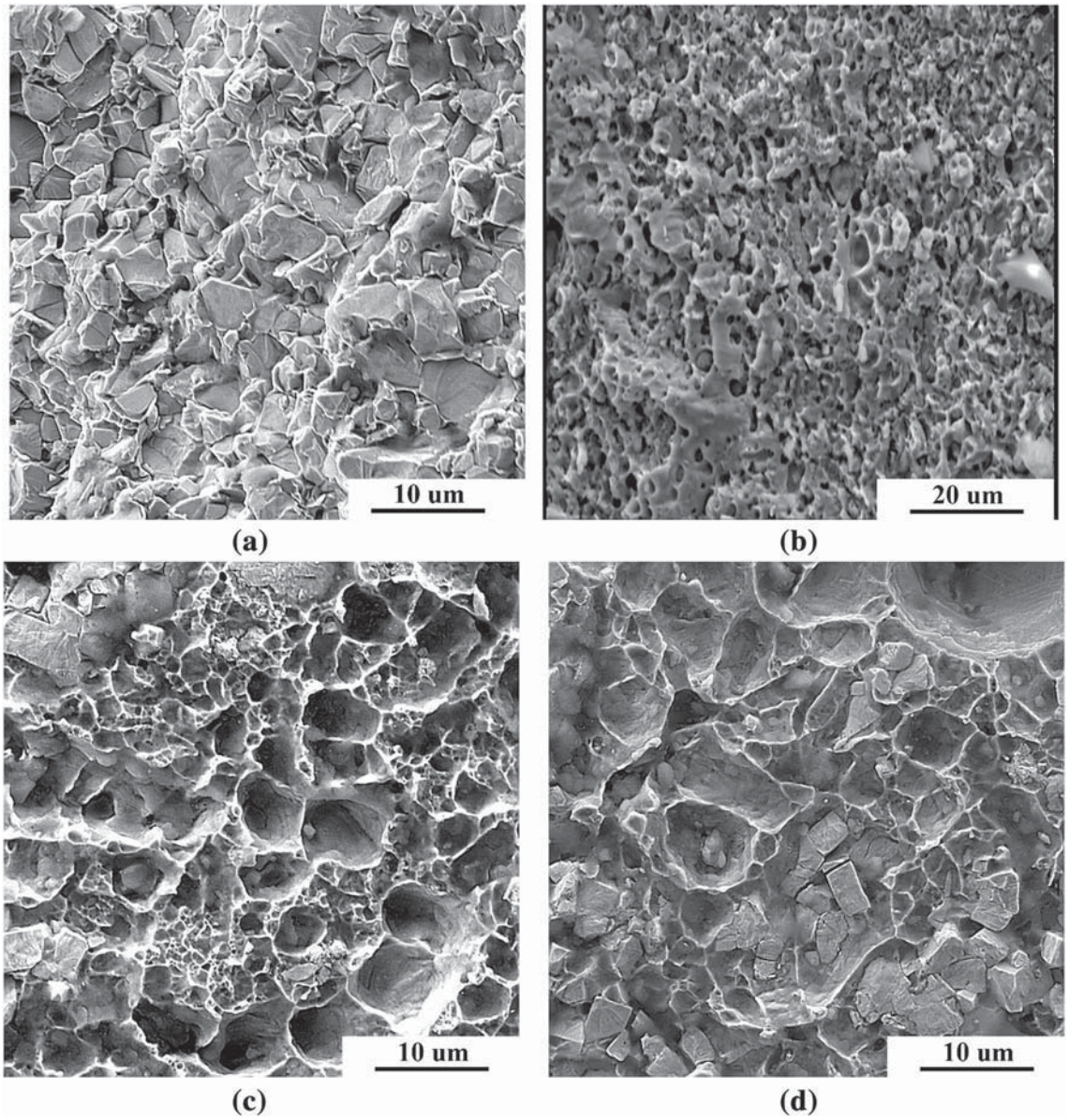

Fig. 9 Fracture surface of the specimens, **a** 930 °C, **b** 960 °C, **c** 990 °C, **d** 1020 °C

made at 930 °C. Presence of WC and Co along with small peaks of α phase indicate low atomic diffusion in this sample. With increase in bonding temperature to 960 °C, WC, α and β phases are detected in the spectrum. Moreover, there are some weak peak intensities implicating restricted formation of Co_3W_3C (η) at the interface. The XRD patterns for the bonds made at higher temperature values are similar to the bond made at 960 °C, as inferred from the intensity of detected peaks for Co_3W_3C (η). This reveals that the formation of this brittle intermetallic compound at higher temperature can be more preferred than that of the joint made at 960 °C. It is suggested that the brazing process in higher temperature values (990 and 1020 °C) intensifies the decomposition of WC particles to W and C elements and permits the easy formation of Co_3W_3C (η) in the joint zone [30]. So uncontrollable propagation of this intermetallic compound in the joint zone lead to the deterioration in mechanical properties (see Fig. 8).

4 Conclusion

Diffusion brazing of 4145 steel to WC–Co cemented carbide using Cu–Zn–Ni interlayer was performed successfully. With increase in bonding temperature, the elements readily diffused across the joint zone and formed various solid solution phases (γ, α and β) and Co_3W_3C intermetallic compound. Moreover, The SEM micrographs

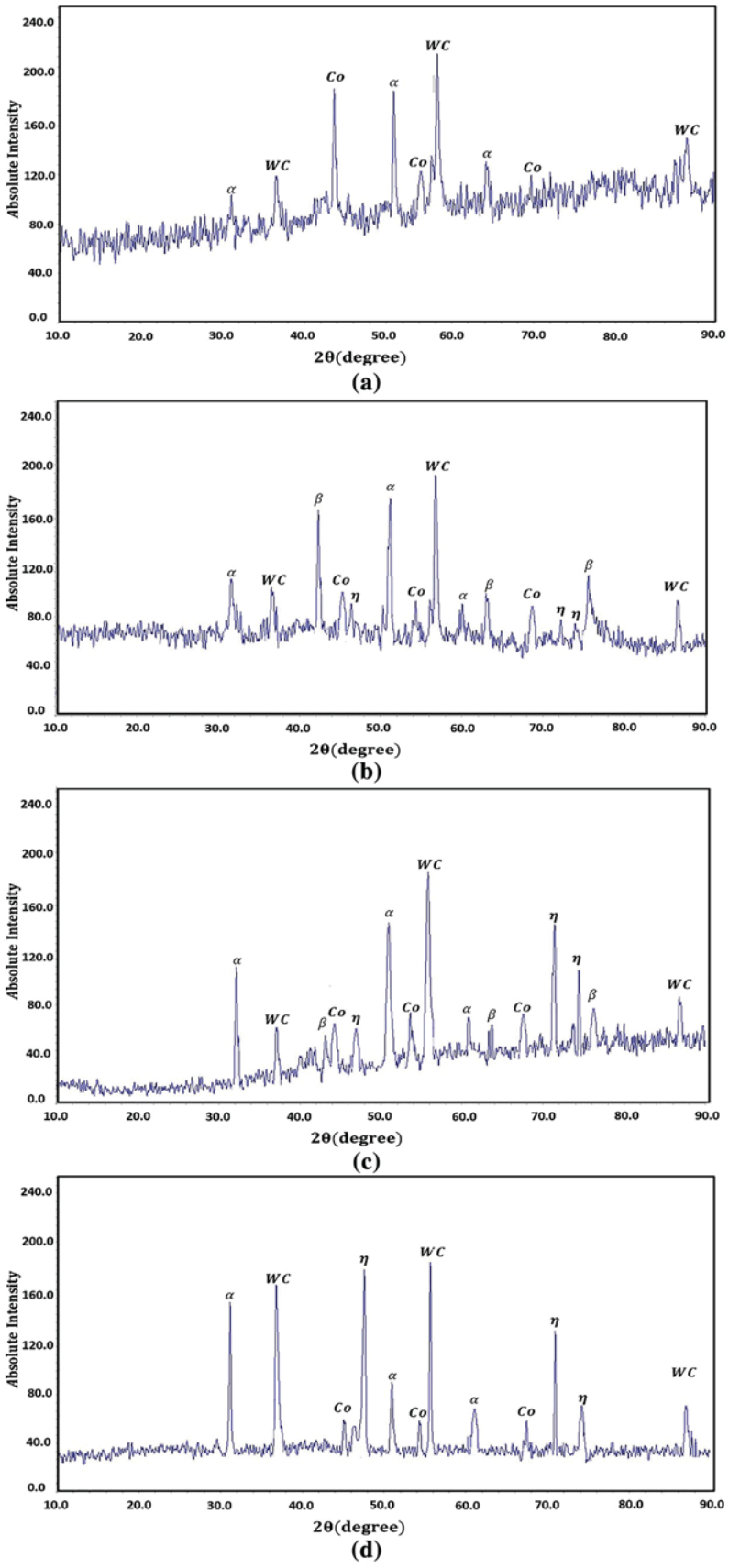

Fig. 10 XRD spectrum for the bonds made at **a** 930 °C, **b** 960 °C, **c** 990 °C, **d** 1020 °C

revealed that with the increase of bonding temperature, the linear shape of interface at WC–Co side changed to a non-linear structure which was due to atomic inter-diffusion across the joint zone. Co dissolution into the interlayer led to the release of WC particles at the interface. The maximum shear strength of 425 MPa was obtained for the bond made at 960 °C. With increase of bonding temperature to higher values, a decrease in the strength occurred which owed to the zinc evaporation, voids formation and interface heterogeneity.

Acknowledgements We thank Taradis Tabesh Azma and CylinderSazi Tehran companies for support of this research.

References

1. Cui X, Wang D, and Guo J, *Int J Mech Sci* **114** (2016) 52.
2. Hua L, Jian S, Chun L, Hong H, Lizhao Q, and Qing L, *J Alloys Compd* **682** (2016) 531.
3. Tarragó J, Coureaux D, Torres Y, Casellas D, Al-Dawerye I, Schneidere L, and Llanes L, *Mater Des* **97** (2016) 492.
4. Appleby-Thomas G, Hazell P, Stennett C, Cooper G, Helaar K, and Diederen A, *J Appl Phys* **105** (2009) 1.
5. Merino-Pérez H, Hodzic A, Merson E, and Ayvar-Soberanisd S, *Compos Struct* **123** (2015) 30.
6. Klünsner T, Zielbauer F, Marsoner S, Deller M, Morstein M, and Mitterer C, *Int J Refract Met Hard Mater* **57** (2016) 24.
7. Shuja S, Yilbas B, Ali H, and Karatas C, *Opt Laser Technol* **86** (2016) 126.
8. Wang H, Yang D, Zhao X, Chen C, and Wang Q, *Sci Technol Weld Join* **10** (2005) 167.
9. Xu P, Ren J, Zhang P, Gong H, and Yang S, *J Mater Eng Perform* **22** (2013) 613.
10. Yu X, Zhou D, Yao D, Lu F, and Xu P, *Int J Refract Met Hard Mater* **56** (2016) 76.
11. Chen G, Zhang B, Wu Z, Mao W, and Feng J, *Int J Refract Met Hard Mater* **40** (2013) 58.
12. Guo Y, Wang Y, Gao B, Shi Z, and Yuan Z, *Ceram Int* **42** (2016) 16729.
13. Feng K, Chen H, Xiong J, and Guo Z, *Mater Des* **46** (2013) 622.
14. Zhou D, Cui H, Xu P, and Lu F, *J Mater Eng Perform* **25** (2016) 2500.
15. Guo Y, Gao B, Liu G, Zhou T, and Qiao G, *Int J Refract Met Hard Mater* **51** (2015) 250.
16. Iamboliev T, Valkanov S, and Atanasova S, *Int J Refract Met Hard Mater* **37** (2013) 90.
17. Tian-en Y, Li Y, Ji X, Lan S, Zhi-xing G, and Xiao-ming Z, *J Cent South Univ* **21** (2014) 2991.
18. Barrenan M, Gómez de Salazar J, and Gómez-Vacas M, *Ceram Int* **40** (2014) 10557.
19. Nowacki J, and Kawiak M, *J Mater Process Technol* **143** (2003) 294.
20. Jiang C, Chen H, Wang Q, Li Y, *J Mater Process Technol* **229** (2016) 562.
21. Li Y, Zhu Z, He Y, Chen H, Jiang C, Han D, and Li J, *J Mater Process Technol* **238** (2016) 15.
22. Chen H, Feng K, Wei S, Xiong J, Guo Z, and Wang H, *Int J Refract Met Hard Mater* **33** (2012) 70.
23. Sui Y, Luo H, Lv Y, Wei F, Qi J, He Y, Meng Q, and Sun Z, *Weld World* **60** (2016) 1269.
24. Samavatian M, Khodabandeh A, Halvaee A, and Amadeh A, *Trans Nonferrous Met Soc China* **25** (2015) 770.
25. Song G, An G, and Liu L, *Mater Des* **35** (2012) 323.
26. Zhang J, Zhang X, Zhou Y, Naka M, and Svetlan A, *Mater Sci Eng A* **495** (2008) 271.
27. Vander Voort G, ASM Handbook, Metallography and Microstructures, vol. 9, ASM International, Almere (2004).
28. ASTM standard D1002, Standard Test Method for Apparent Shear Strength of Singlelap-joint Adhesively Bonded Metal Specimens by Tension Loading (Metal-to-metal), ASTM International, Almere (1999).
29. Baker H, Alloy phase diagrams, ASM International, vol. 3, ASM Handbook (2004).
30. Lee W, Kwon B, and Jung S, *Int J Refract Met Hard Mater* **24** (2006) 215.